Journal of Power Sources 199 (2012) 256–262

Contents lists available at SciVerse ScienceDirect

Journal of Power Sources

journal homepage: www.elsevier.com/locate/jpowsour

High-rate capability of $LiFePO_4$ cathode materials containing Fe_2P and trace carbon

Yuehui Yin [a], Mingxia Gao [a,*], Hongge Pan [a], Lukai Shen [a], Xin Ye [a], Yongfeng Liu [a], Peter S. Fedkiw [b], Xiangwu Zhang [c]

[a] State Key Laboratory of Silicon Materials, Department of Materials Science and Engineering, Zhejiang University, Hangzhou 310027, PR China
[b] Department of Chemical and Biomolecular Engineering, North Carolina State University, Raleigh, NC 27695-7905, USA
[c] Fiber and Polymer Science Program, Department of Textile Engineering, Chemistry and Science, North Carolina State University, Raleigh, NC 27695-8301, USA

ARTICLE INFO

Article history:
Received 16 November 2010
Received in revised form 5 July 2011
Accepted 11 October 2011
Available online 20 October 2011

Keywords:
Lithium-ion battery
Lithium iron phosphate
Particle size
Rate capability
Mechanical activation

ABSTRACT

Carbon coating and nano-scale particle size are two impactful factors in improving the rate capability of $LiFePO_4$ cathode materials for lithium-ion batteries. However, both factors decrease the tap density of the materials and are possibly causing unfavorable effect on the volumetric capacity of the cathode materials and thus the batteries, which is undesirable in commercial application. In the present study, $LiFePO_4$ materials with moderate particle size of sub-micron and trace carbon content (0.5–0.9 wt.%) are synthesized by a mechanical activation method. High-electronic conductivity iron phosphides (Fe_2P/FeP) are in situ introduced into the $LiFePO_4$ materials and the amount is modified by the calcination temperature. Electrochemical testing shows that Fe_2P/FeP plays an important role in improving the high-rate capability of $LiFePO_4$ with moderate particle size. The product calcined at 700 °C, which has a high-tap density of 1.37 g cm^{-3} correlating to a specific surface area approximately of 4 m^2 g^{-1}, possesses discharge capacities of 110 and 100 mAh g^{-1} at discharge rates of 5 C and 10 C, respectively. The introduction of Fe_2P/FeP in an amount of ca. 5 wt.% rather than carbon coating and the moderate particle size of $LiFePO_4$ are promising approaches to obtain $LiFePO_4$ cathode material of high-rate capability without unduly compromising its volumetric capacity.

1. Introduction

Since the pioneering work of Padhi et al. [1], olivine-type $LiFePO_4$, as a promising cathode material for lithium-ion rechargeable battery, has attracted wide attention due to its well-known advantages of good cycling stability, low cost, low toxicity, appropriate potential of lithium-ion insertion/extraction (ca. 3.45 V vs. Li^+/Li), high theoretical capacity (ca. 170 mAh g^{-1}), and thermal stability, and so on. However, its low-electronic conductivity (ca. 10^{-9} S cm^{-1}) [1,2] stemming from the polyoxyanion structure as well as the low lithium-ion diffusivity within particles (ca. 10^{-16}–10^{-14} cm^2 s^{-1}) [3,4] result in a poor rate capability, and hence prevent it from being applied more widely, e.g. in hybrid and plug-in hybrid electric vehicles. Therefore, extensive research has been carried out, and remarkable progress has been achieved in the past decade. Effective approaches in improving the rate capability of $LiFePO_4$ cathode materials include: coating $LiFePO_4$ particles with a carbon layer to enhance the electronic conductivity, which can also restrain the grain growth of $LiFePO_4$ [5–7]; minimizing particle size to nano-scale so as to reduce the lithium-ion diffusion path [7–9]; and doping $LiFePO_4$ with super-valence cations [10–13], which can enhance the electronic conductivity. Moreover, in many cases, carbon coating and particles minimization to nano scale are simultaneously adopted [7–9,14].

However, nano-size particles commonly lead to low-tap density and make electrode fabrication more difficult than micron size particles [15]. Particle fining may decrease the volumetric energy density of the battery cell because the dense packing of the fine particles is practically difficult and low packing density is one of the disadvantages of carbon materials [16]. And for carbon coating, Dahn and coworkers [17] demonstrated that even 3 wt.% of carbon coating decreased the tap density of $LiFePO_4$ by over 40%. Therefore, it is necessary to prepare $LiFePO_4$ of high-rate capability with moderate particle size and low-carbon content, in order to avoid the unfavorable effect on its volumetric capacity.

Fe_2P has a high-electronic conductivity of 10^{-1} S cm^{-1} [18]. FeP is also a high-electronic conductivity phase. The formation of iron phosphide (Fe_2P) and/or iron phosphocarbides ($Fe_{75}P_{15}C_{10}$) at the grain boundaries of $LiFePO_4$ demonstrated a significant increase of the electronic conductivity of the $LiFePO_4$ material up to ca. 10^{-2} S cm^{-1} [19]. It is also reported that in the $LiFePO_4$/C (3–5 wt.% carbon) materials, the presence of 4–7 wt.% Fe_2P improved the

* Corresponding author. Tel.: +86 571 87952615; fax: +86 571 87952615.
E-mail address: gaomx@zju.edu.cn (M. Gao).

0378-7753/$ – see front matter © 2011 Elsevier B.V. All rights reserved.
doi:10.1016/j.jpowsour.2011.10.042

electronic conductivity of the materials by 4 order of magnitudes [19]. But its amount should be carefully controlled [20,21], as Fe_2P is an inactive phase for lithium-ion insertion/extraction, and other impurity phases also formed along with the formation of Fe_2P, such as Li_3PO_4.

In the present work, $LiFePO_4$ materials with trace carbon and sub-micron particle size rather than nano-size were synthesized by a mechanical activation method. High-electronic conductivity phases of Fe_2P as well as trace FeP were in situ introduced into the $LiFePO_4$ products. The amount of Fe_2P and the particle size of $LiFePO_4$ were adjusted by the calcination temperature. The structure and the electrochemical properties of the products were studied. As the Fe_2P phase has a high density of 6.8 g cm^{-3}, which is much higher than that of $LiFePO_4$ (3.6 g cm^{-3}) and carbon bulk (2.2 g cm^{-3}), the introduction of Fe_2P rather than sufficient carbon coating is considered promising in getting $LiFePO_4$ materials of high-tap density. The results are hopefully helpful in the fabrication of $LiFePO_4$ materials with high-rate capability without unduly deteriorating its volumetric capacity.

2. Experimental

Li_2CO_3, $FeC_2O_4{\cdot}2H_2O$ and $NH_4H_2PO_4$ (chemicals purity >99%) were used as starting materials. These starting materials in amounts based on the stoichiometric composition of $LiFePO_4$ were dispersed in acetone, and then were ball milled for 3 h with a ball-to-powder weight ratio of 10:1 and a rotation speed of 300 rpm by using a planetary mill. The resulting suspension was pre-treated by heating at 350 °C for 10 h under Ar atmosphere and followed by another ball milling of 1 h in Ar. The ball milled precursor was then calcined at temperatures of 550, 600, 700 and 800 °C, respectively, for 10 h in a reductive atmosphere of N_2 + 5 vol% H_2, forming $LiFePO_4$ products. A heating rate of 10 °C min^{-1} and a natural cooling in the furnace were adopted in the calcination process. The $LiFePO_4$ products were further ground by mortar and pestle to powders for structural characterization and electrochemical testing.

The morphology of the $LiFePO_4$ products was observed by scanning electron microscopy (SEM, Sirion-100, FEI). The phase identification of the products was carried out by X-ray diffraction (X'Pert PRO, PANalytical) using Cu Kα radiation (λ = 1.54056 Å) by a step scanning method with a step interval of 0.02° and a count time of 1 s per step. The lattice parameters of $LiFePO_4$ and the phase composition of the products were analyzed by a Rietveld refinement method. Crystallite size of $LiFePO_4$ was calculated by Debye–Scherrer equation. The carbon content of the products was measured by an elemental analyzer (Flash EA 1112, ThermoFinnigan). The specific surface area measurement of the products was conducted by a BET (Brunauer–Emmett–Teller) method (Autosorb-1-c, Quantachrome) and the particle size distribution was measured using a particle size distribution analyzer (LS13 320, Beckman Coulter). The tap density was tested by adding a determinate quantity of the $LiFePO_4$ powder into a measuring cylinder, and then continually tapping the cylinder on a table until the volume of the powder cannot be changed. The ratio of the mass to the final volume of the powder was taken as the tap density.

Electrochemical testing was carried out by coin cells of CR2025 with Li foil as anode and counter electrode and a microporous polyethylene sheet (Celgard 2400, Celgard) as separator. The cathodes were prepared by blending the $LiFePO_4$ product, acetylene black and polyvinylidene fluoride (PVDF) in a weight ratio of 75:15:10 in N-methyl-pyrolidinone forming a slurry, and subsequently pasting the slurry on an Al foil, followed by a heating at 120 °C for 14 h under vacuum. Then the foil was punched to disks in a diameter of 14 mm, and then pressed at 6 MPa at room temperature for 30 s. Packing density of the $LiFePO_4$ cathode coating

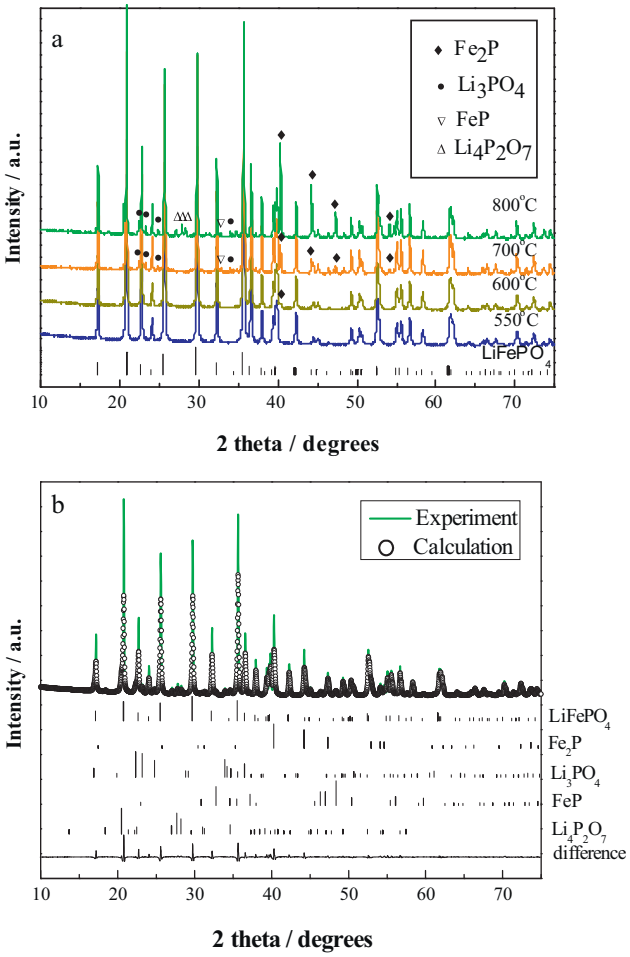

Fig. 1. (a) XRD patterns of the $LiFePO_4$ products synthesized at different calcination temperatures, (b) A representative XRD Rietveld analysis pattern, which is from the sample calcined at 800 °C.

was obtained by measuring the mass density of the cathode coating including the $LiFePO_4$ material, the binder and the conductive additive of acetylene black electron at the same pressing and drying state used for the cell for the electrochemical property testing. A typical cathode disk contained ca. 3.6 mg cm^{-2} of the $LiFePO_4$ product. A solution of 1 M $LiPF_6$ with ethylene carbonate (EC)/dimethyl carbonate (DMC) (1:1 by volume) was used as the electrolyte. The cells were assembled in a glove box (Labstar, Braun) filled with high-purity Ar.

The cells were galvanostatically cycled in a potential range of 2.0–4.3 V vs. Li/Li$^+$ with different discharge rates and a same charge rate of 0.1 C (1 C = 170 mA g^{-1}). Electrochemical impedance spectra (EIS) measurements were performed using a frequency response analyzer (Solartron 1255B, Solartron) equipped with an electrochemical interface (1287, Solartron) in a frequency range of 100 kHz to 0.01 Hz and a potentiostatic signal amplitude of 5 mV. Prior to the EIS measurements, cells were first activated by four cycles at 0.1 C between 2.0 V and 4.3 V vs. Li/Li$^+$, then polarized to 3.4 V and maintained the potential for 2 h. All of the electrochemical tests were performed at 25 °C.

3. Results and discussion

3.1. Structure characteristics

Fig. 1(a) shows the XRD patterns of all the products calcined at different temperatures. It is seen that $LiFePO_4$ with orthorhombic

Table 1
The phase composition of the products and the lattice parameters and the crystallite size of the $LiFePO_4$ obtained at different calcination temperatures.

Calcination temperatures (°C)	Lattice parameters (Å)			Crystallite size (1 3 1) facet (nm)	Phase content (wt.%)				
	a	*b*	*c*		$LiFePO_4$	Fe_2P	FeP	Li_3PO_4	$Li_4P_2O_7$
550	10.326	6.008	4.695	40.6	100.0	/	/	/	/
600	10.326	6.008	4.695	45.7	99.3	0.7	/	/	/
700	10.324	6.006	4.694	70.3	91.2	3.7	1.4	3.6	/
800	10.322	6.006	4.694	75.0	76.0	11.3	1.7	4.8	6.1

Fitting satisfaction: $R_w/R_{exp} < 5\%$, $R_w < 10\%$.

structure and a space group of *Pnma* is the main phase of all the products. The sharp peaks indicate that the phases formed in the products are of good crystallinity. The phase composition of the products and the lattice parameters of $LiFePO_4$ calculated by the Rietveld refinement method are listed in Table 1. A representative XRD Rietveld analysis pattern, which is from the sample calcined at 800 °C, is displayed in Fig. 1(b). No detectable effect of the calcination temperature on the lattice parameters of $LiFePO_4$ is observed. The lattice parameters are very close to those given in the JCPDS card (No. 40-1499, $a = 10.334$, $b = 6.010$, $c = 4.693$). However, the crystallite size ((1 3 1) facet) of $LiFePO_4$ increases from 40.5 nm to 75.0 nm as the calcination temperature increased from 550 to 800 °C, especially, showing a jumping increase as the calcination temperature increased from 600 to 700 °C.

From Fig. 1(a) and Table 1, it is seen that $LiFePO_4$ is the only phase detected in the product calcined at 550 °C by XRD. Fe_2P starts to form at 600 °C, and its amount increases with the calcination temperature, from 0.7 to 3.7 wt.% as the calcination temperature increases from 600 to 700 °C, further reaching a high value of 11.3 wt.% when the calcination temperature is 800 °C. Minor amount of FeP also formed at the calcination temperatures of 700 and 800 °C. Additionally, considerable amounts of Li_3PO_4 and $Li_4P_2O_7$ impurities formed in the product calcined at 800 °C.

According to the element analysis, only trace carbon ranging from 0.9 to 0.5 wt.%, corresponding to the increase of the calcination temperature from 550 to 800 °C, existed in the products, which is reliable as no especial carbon source was added in the synthesis process. In this case, the unfavorable negative effect from the carbon on the tap density of $LiFePO_4$ is hopefully diminished. The typical morphologies of the $LiFePO_4$ products calcined at different temperatures are displayed in Fig. 2. Fig. 2(a) and (b) shows that the morphologies of the products calcined at 550 and 600 °C are not visibly different, which displays as the agglomeration of several small primary $LiFePO_4$ particles that form large secondary particles. Moreover, as seen from Fig. 2(b) and (c), the primary particles of $LiFePO_4$ grew when the calcination temperature was increased from 600 to 700 °C, and agglomeration also exists. The primary particles grew further but the agglomeration reduced when the calcination temperature was further increased to 800 °C, Fig. 2(d). By the further analyses of both the size distribution (Fig. 3) and the mean diameter as well as the specific surface area of the particles (Table 2), it is seen that the apparent particle size increases with the calcination temperature increasing from 600 to 700 °C. Though the SEM images of the samples calcined at 550 and 600 °C are not visibly different, Fig. 3 and Table 2 show that the mean particle size of the sample calcined at 600 °C is slightly larger than that of the sample calcined at 550 °C. The mean particle size increases monotonically,

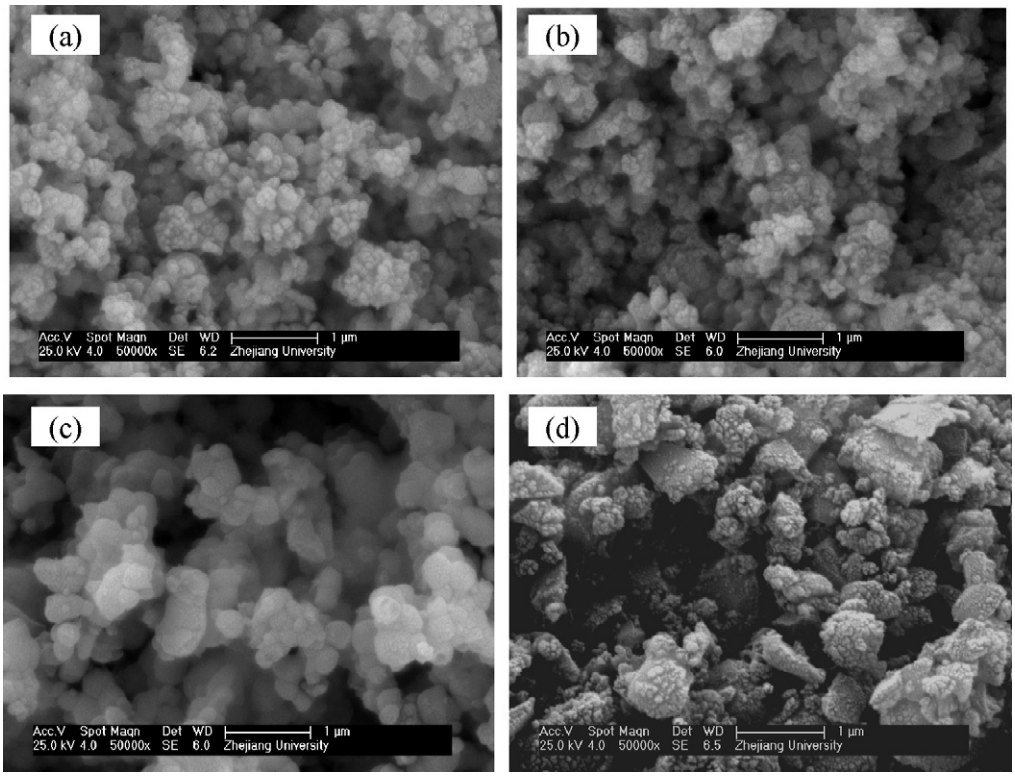

Fig. 2. SEM images of the $LiFePO_4$ products calcined at temperatures of (a) 550 °C, (b) 600 °C, (c) 700 °C, and (d) 800 °C.

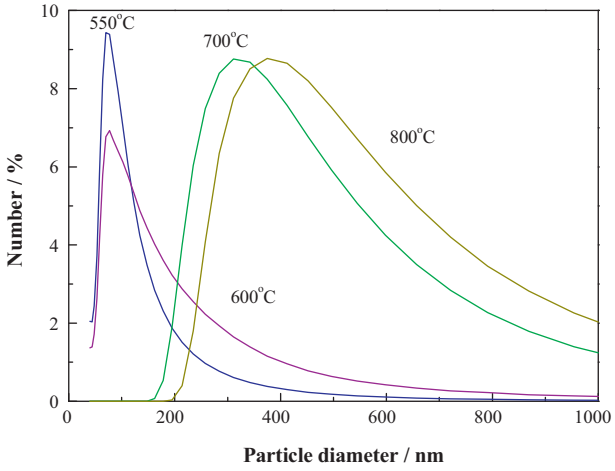

Fig. 3. The particle size distribution of the $LiFePO_4$ products calcined at temperatures of 550–800 °C.

and accordingly the specific surface area decreases, with increase of calcination temperature. Moreover, two distinguishable ranges of the particle size distribution are seen from Fig. 3 and Table 2. One is the smaller mean diameter range of 115–160 nm corresponding to the calcination temperature range of 550–600 °C, and the other is the larger mean diameter range of 482–575 nm corresponding to the calcination temperature range of 700–800 °C.

The present product calcined at 700 °C displays a particle size of sub-micron and a low specific surface area of 4 $m^2\,g^{-1}$. Its tap density is 1.37 g cm^{-3}, which is comparatively higher than that of the $LiFePO_4$ materials with nanoparticles and an irregular carbon coating, being of less than 1.0 g cm^{-3} [22]. Another literature publication showed that the tap density is 1.12 g cm^{-3} for a spherical $LiFePO_4$/C with a specific surface area of 41.37 $m^2\,g^{-1}$ [23]. As the particle size was not reported for this material, some results from the literature that $LiFePO_4$/C particles with particle size of 30–100 nm had a specific surface area of 98.3 $m^2\,g^{-1}$ [14] and a $LiFePO_4$/C material with particle size of 250 nm had a specific surface area of 12.1 $m^2\,g^{-1}$ [24] may can provide some information on the correlation between the specific surface area and the particle size.

3.2. Electrochemical properties

Fig. 4(a) illustrates the electrochemical impedance curves of the $LiFePO_4$ products calcined at different temperatures. The solid symbols denote the experimental data, and the lines represent the fitting results which is from the calculation based on the equivalent circuit [25] displayed in Fig. 4(b). The inset of Fig. 4(a) is the amplification of the high frequency region. The intercept of the curve at high frequency at the real axis relates to the bulk resistance of electrolyte (R_e). The two depressed semicircles in the medium-high and medium-low frequency region relate to the resistance from the solid–electrolyte interface film of the surface of the cathode (R_{film}) and the charge-transfer resistance (R_{ct}) at the particle surfaces,

Table 2
The specific surface area and the mean diameter of the particles of the $LiFePO_4$ products calcined at different temperatures.

Calcination temperatures (°C)	Mean diameter (nm)	Specific surface area ($m^2\,g^{-1}$)
550	115	10.57
600	160	7.99
700	482	4.05
800	575	2.52

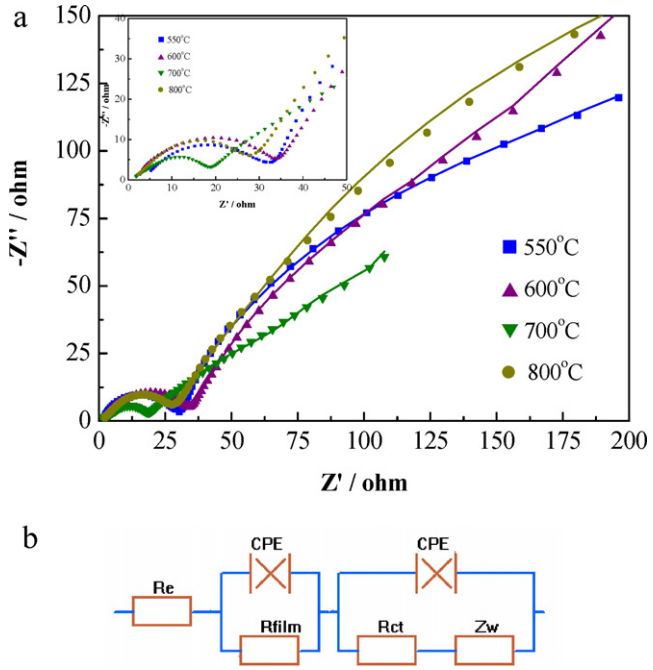

Fig. 4. (a) Electrochemical impedance curves of the $LiFePO_4$ products calcined at different temperatures. The solid symbols denote the experimental data, and the lines represent the fitting results from the calculation based on the equivalent circuit (b). The inset of (a) is the amplification of the experimental data in high frequency region.

respectively, as referred by [26], of which a larger partial radius relates to a larger resistance. The straight line in the low-frequency region, namely the Warburg resistance Z_w, is attributed to the diffusion resistance of lithium ions within the $LiFePO_4$ particles. By using the equivalent circuit (Fig. 4(b)), where CPE (the constant phase elements) denotes the double-layer capacitance, and by using the Zplot® software, the R_{ct} values of the products were obtained as 171, 132, 35 and 434 Ω for the calcination temperatures of 550, 600, 700 and 800 °C, respectively.

The value of R_{ct} of the $LiFePO_4$ materials decreases from 171 to 35 Ω with increase of the calcination temperature from 550 to 700 °C, but the trend reverses and the values of R_{ct} increases to 434 Ω when the calcination temperature is further increased to 800 °C. The considerably lowest value of R_{ct} of the $LiFePO_4$ product calcined at 700 °C indicates that the product possesses the best reaction kinetics of lithium-ion insertion and extraction during electrochemical cycling. Combining the results of the structure and morphology features of the products discussed above, it is suggested that the reduction of charge-transfer resistance of the products with calcination temperature increasing from 550 to 700 °C should be due mainly to the formation and the appropriate amount of Fe_2P/FeP, despite the increase of particle size of $LiFePO_4$. However, the reaction kinetics deteriorate severely for the product calcined at 800 °C because of the presence of the large amount of impurity phases Li_3PO_4 and $Li_4P_2O_7$ formed along with the high content of Fe_2P, which have much lower electronic and lithium-ion conductivity than that of $LiFePO_4$ [27,28], and the increased particle size of $LiFePO_4$.

Fig. 5(a)–(c) illustrates the charge/discharge curves of the first cycle of the $LiFePO_4$ products at discharge rates of 0.1, 1 and 5 C, respectively. Fig. 5(a) shows that at the low-discharge rate of 0.1 C, the difference of the potentials between the charge and discharge plateaus (vs. Li/Li^+) is small for the products calcined at different temperatures. Though the sample calcined at 700 °C has higher capacity than the others, the potential difference is only neglectably smaller compared with that of the other samples. However, with

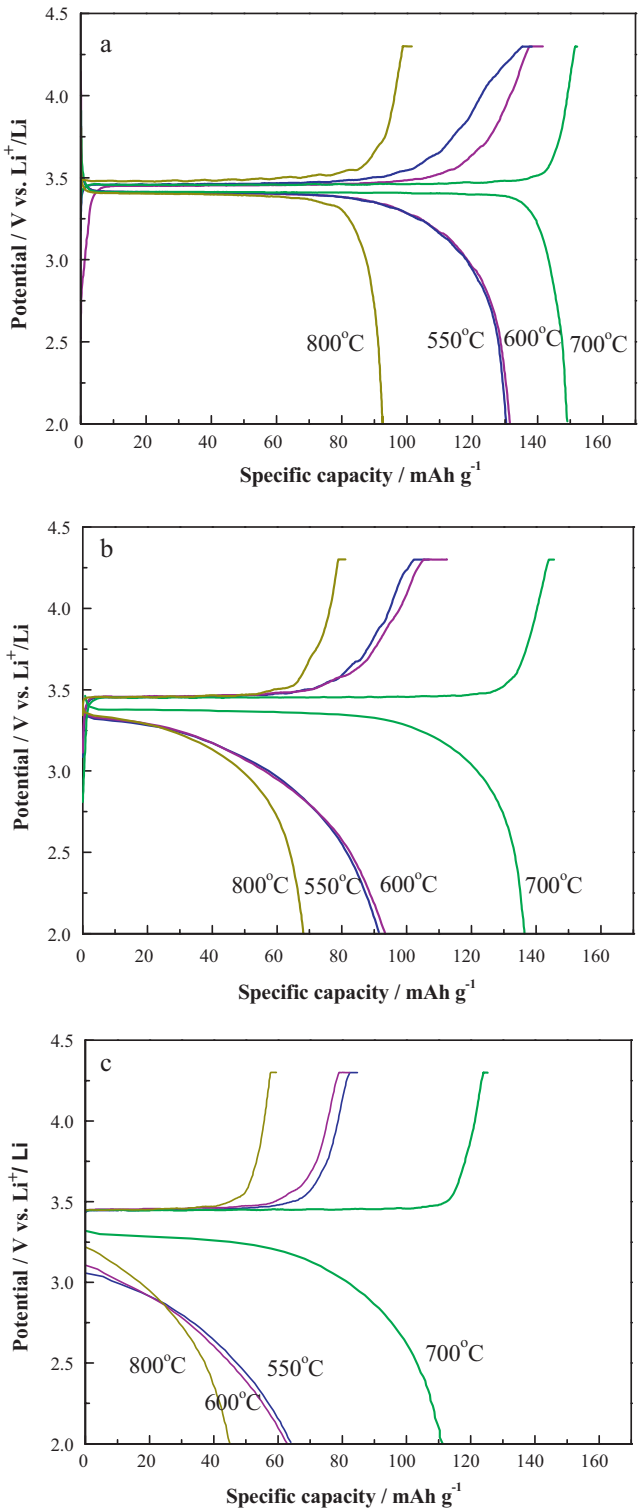

Fig. 5. The charge and discharge curves of the first cycle of the $LiFePO_4$ products calcined at different temperatures at charge rates of (a) 0.1 C, (b) 1 C and (c) 5 C.

the increase of the discharge rate, the charge and discharge potential difference increases as seen in Fig. 5(b) and (c). The potential difference between the charge and discharge plateaus correlates an import electrochemical phenomenon denoted as electrochemical polarization, which is an important factor in evaluating the electrode reaction kinetics during cycling. Electrochemical polarization is the deviation of the electrode potential from the steady-state potential that the electrode exhibits in the absence of an external current. If only one electrode reaction is possible at the electrode, then steady-state potential coincides with the equilibrium potential of the reaction, and the electrochemical polarization corresponds to the excess voltage of the reaction. For lithium-ion batteries, both lithium ion and electrons transfer between the anode and the cathode during cyclying. At the discharge process, lithium-ions extract from $LiFePO_4$, and the electrons move towards $LiFePO_4$ cathode, if the cathode reaction which corresponds to the extraction of the lithium-ions cannot consume these electrons, then the un-consumed electrons concentrate at the cathode, thus a cathodic polarization occurs. For compensation, the reaction occurs towards lower potential, resulting in a decline of the discharge plateaus, which shows a larger negative deviation from equilibrium potential of the reaction. Similarly, if un-consumed lithium ions concentrate at the cathode during charge, a positive deviation of the discharge plateaus would also occurs. It is well known that the polarization of $LiFePO_4$ cathode during the charge process is not severe, as is also seen in Fig. 5. Therefore, the larger difference between the charge and the discharge plateaus, the severer polarization of the electrode, is caused by the discharge reaction of $LiFePO_4$. Less polarization correlates a better reaction kinetics. Combining Fig. 5, and the corresponding calcination temperature and hence the structure of the samples, it is seen that the variation of the polarization with the discharge rate correlates with the calcination temperature, which in turn correlates with particle size and Fe_2P/FeP content. Relative to the other products, the sample calcined at 700 °C shows a slight increase in the potential differences with increasing the discharge rate from 0.1 C to 5 C, as shown in Fig. 5(a)–(c). This indicates that the polarization of the product calcined at 700 °C is only slightly severer, while that of the products calcined at 550, 600 and 800 °C become much severer, with the increase of the high-discharge rates. Thus, it is believed that the appropriate amount of Fe_2P/FeP (ca. 5 wt.%) contributed greatly to the high reaction kinetics of the product calcined at 700 °C, which has moderate particle size of $LiFePO_4$. Whereas either trace amount of Fe_2P even with smaller particle size of $LiFePO_4$ (as for the product calcined at 600 °C) or high amount of Fe_2P but with larger particle size of $LiFePO_4$ (as for the produce calcined at 800 °C) do not result in good reaction kinetics for the $LiFePO_4$ materials.

In addition, it is worth to note that the $LiFePO_4$ product calcined at 800 °C has the lowest capacity at 0.1 to 5C (Fig. 5), but its discharge plateau potential at 1 C rate is close to that of the samples calcined at 550 °C and 600 °C, even a bit higher (Fig. 5(b)). However, the discharge plateau (though not flat) potential of the sample calcined at 800 °C tends to be higher than that of those calcined at 550 and 600 °C at the discharge rate of 5 C (Fig. 5(c)), showing a reversed situation compared with that in Fig. 5(b). This indicates that the polarization of the product calcined at 800 °C is less severe than that of those calcined at 550 and 600 °C when the discharge rate is increased from 1 to 5 C, despite the former has larger particle size and high amount inactive phases of Li_3PO_4 and $Li_4P_2O_7$. This suggests that suitably higher Fe_2P (Table 1) plays much important role in improving the reaction kinetics of $LiFePO_4$ with increase of the discharge rate to a high level, such as up to 5 C.

The discharge capacities of the samples calcined at different temperatures at discharge rates from 0.1 to 15 C are illustrated in Fig. 6. It is seen that the product calcined at 700 °C possesses the highest discharge capacity among all of the products at any discharge rates: ca. 149 mAh g^{-1} at 0.1 C; 136 mAh g^{-1} at 1 C; 110 mAh g^{-1} at 5 C; and 100 mAh g^{-1} at 10 C. The products calcined at 550 and 600 °C show very close discharge capacity, and the capacity is higher than that of the product calcined at 800 °C up to 10 C. But when the discharge rate is further increased to 15 C, the Fe_2P-containing samples, either the sample calcined at 600 °C with trace amount of Fe_2P and thus high content of $LiFePO_4$, or calcined at 800 °C with large amount of Fe_2P and thus low content

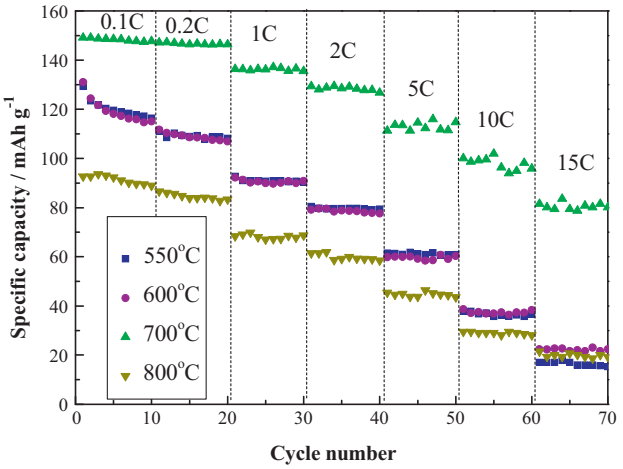

Fig. 6. The capacity of the $LiFePO_4$ products calcined at different temperatures at different discharge rates from 0.1 C to 15 C.

of $LiFePO_4$, possess higher capacity than the product without Fe_2P, the one calcined at 550 °C. Therefore, it is concluded that even trace Fe_2P has favorable effect on the high-rate capability of the $LiFePO_4$ materials with moderate particle size and trace carbon, and suitable amount of Fe_2P is a key factor in improving the high-rate performance. However, too much Fe_2P deteriorates the electrochemical capacity of the cell as it results in lower content of active material of $LiFePO_4$. Though the capacity of 149 mAh g^{-1} for the product calcined at 700 °C is not so favorable for the 0.1 C rate discharge, the capacities of 110 mAh g^{-1} at 5 C and 100 mAh g^{-1} at 10 C are considerably favorable. It was pointed out that the in situ formed Fe_2P was mainly distributed on the boundary of the $LiFePO_4$ particles [21], hence the electronic conductivity of the $LiFePO_4$ materials is effectively enhanced and the rate capability is improved.

Although results from different laboratories cannot be quantitatively compared because of different electrode preparation and testing programs, it is still useful to observe progress made among the research communities. The loading of the $LiFePO_4$ coating is also an important factor for the apparent electrochemical performance in the manner that a thinner loading leads to a better appearant rate performance. Therefore, the follow brief review of the electrochemical performance of $LiFePO_4$ with different particle size, carbon coating, specific surface area, etc. from different laboratories also includes the loading condition of the $LiFePO_4$ coating of the cathodes. A carbon-coated pure $LiFePO_4$ with particle size of 200 nm is reported to have achieved a high capacity of 160 mAh g^{-1} at 0.1 C, however, the capacity dramatically decreased to 63 mAh g^{-1} at 4 C [29], but the loading of the $LiFePO_4$ coating was not presented. A cathode of $LiFePO_4$/C (1.4 wt.% carbon) with a primary particle size of 100–200 nm in an loading of 7.0 mg cm^{-2} possess a capacity of 118 mAh g^{-1} at 10 C rate [16]. Pure $LiFePO_4$ with a comparable particle size to our present study was reported possessing a high capacity of 165 mAh g^{-1} at 0.1 C in the case of the $LiFePO_4$ loading being of 3.2 mg cm^{-2} [6], but it contained a higher carbon content of 6 wt.%. When the carbon content was decreased to 3.8 wt.%, the capacity at 0.1 C decreased to 136 mAh g^{-1} and the capacity at 2C was only 122 mAh g^{-1}. Comparable or slightly higher capacities at 5 and 10 C rates to the present results for $LiFePO_4$ materials without Fe_2P were also reported, but the material also contained higher content of carbon coating (2.8–6 wt.%) and the $LiFePO_4$ particle size is less than 100 nm [30,31] or 100–300 nm [32]. The cathode material loadings used were 1 and 3–4 mg cm^{-2} in [31] and [32], respectively, which is lower or comparable as the present study. Though the present $LiFePO_4$ material only contains trace carbon and has moderate particle size in ca. 500 nm, combining the above mentioned rate performance from previous works, it is seen that the rate capability of the $LiFePO_4$ material synthesized at the calcination temperature of 700 °C in the present study is promising. The high-rate capability of the $LiFePO_4$ materials is ensured by an appropriate amount of in situ formed Fe_2P. Both the trace carbon content and moderate particle size is beneficial in enhancing the tap density of the $LiFePO_4$ material and is also beneficial for electrode preparation compared with the carbon coated smaller nano-size $LiFePO_4$ materials.

To get an initial estimation of the volumetric energy density of the $LiFePO_4$ cathode material, the values of the one calcined at 700 °C at 0.1 C, 1 C and 5 C were measured, respectively. The packing density of the $LiFePO_4$ coating of the cathode was measured as 1.6 g cm^{-3}. Assuming the middle discharge potential (vs. Li/Li^+), which are of 3.41, 3.36 and 3.21 V for 0.1 C, 1 C and 5 C, respectively, as an average potential, the volumetric energy density of the $LiFePO_4$ coating of the cathode are correspondingly of 813, 731 and 565 mWh cm^{-3}. The thickness of the present $LiFePO_4$ electrode coating is about 30 μm. A previous reported nano-sized (300–400 nm) $LiFePO_4$/C (3.8 wt.%C) coating with a packing density of 2.0 g cm^{-3} possessed capacities of 125 and 100 mAh g^{-1} at 5 C, respectively, with electrode coating thickness being of 20 and 40 μm [33], but the discharge potential was not reported. If taking a similar potential, the present volumetric energy densities at 1 C and 5 C is guesstimated somewhat lower than that in the literature. But the present volumetric energy density at 10 C is guesstimated competitive with that at 8 C in the literature based on their reported value [33]. The study of the volumetric energy density of $LiFePO_4$ material is very rare compared with that of the gravimetric capacity and the corresponding literature is very limited. Additionally, as different testing parameters, such as the electrolyte, packing density and thickness, and cyclic potential range, were used, the above comparison is rough. However, it is expected that the present data could give an initial impression for the volumetric energy density of the $LiFePO_4$ cathode materials.

4. Conclusions

$LiFePO_4$ cathode materials for lithium-ion batteries with trace carbon content (ca. 0.5–0.9 wt.%) and sub-micron particle size were synthesized by a mechanical activation method. High-electronic conductivity phases of Fe_2P as well as FeP were formed in situ in the material and their amount was adjusted by the calcination temperature. Fe_2P/FeP plays important role in improving the high-rate capability of the $LiFePO_4$ materials with moderate particle size and trace carbon. $LiFePO_4$ material with Fe_2P/FeP in an amount of ca. 5 wt.%, which was obtained at a calcination temperature of 700 °C, possesses capacities of 136, 110 and 100 mAh g^{-1} at discharge rates of 1, 5 and 10 C, respectively. The limited carbon content and the moderate particle size result in a high-tap density of 1.37 g cm^{-3} for the $LiFePO_4$ material. High calcination temperature (800 °C) led to too large amount of Fe_2P and impurities and also large-particle size, while low calcination temperature (600 °C) cannot introduce sufficient amount Fe_2P. Both temperatures cannot produce $LiFePO_4$ materials with high rate performance. The introduction of Fe_2P phase rather than carbon coating is expected to be a promising way to improve the high-rate capability of $LiFePO_4$ material without unduly compromising its volumetric capacity.

Acknowledgements

The work was supported by National Natural Science Foundation for Distinguished Young Scholars of PR China (No. 51025102), Science and Technology Program of Zhejiang Province, PR China (No. 2009C34012 and No. 2008C24002) and Natural Science Foundation of Zhejiang Province, PR China (No. Y4080190).

References

[1] A.K. Padhi, K.S. Nanjundaswamy, J.B. Goodenough, Journal of the Electrochemical Society 144 (1997) 1188–1194.
[2] K. Striebel, J. Shim, V. Srinivasan, J. Newman, Journal of the Electrochemical Society 152 (2005) A664–A670.
[3] P.P. Prosini, M. Lisi, D. Zane, M. Pasquali, Solid State Ionics 148 (2002) 45–51.
[4] A. Dell'Era, M. Pasquali, Journal of Solid State Electrochemistry 13 (2009) 849–859.
[5] C.Z. Lu, G.T.K. Fey, H.M. Kao, Journal of Power Sources 189 (2009) 155–162.
[6] J.K. Kim, G. Cheruvally, J.H. Ahn, Journal of Solid State Electrochemistry 12 (2008) 799–805.
[7] J. Ni, M. Morishita, Y. Kawabe, M. Watada, N. Takeichi, T. Sakai, Journal of Power Sources 195 (2010) 2877–2882.
[8] D. Choi, P.N. Kumta, Journal of Power Sources 163 (2007) 1064–1069.
[9] M. Konarova, I. Taniguchi, Journal of Power Sources 195 (2010) 3661–3667.
[10] S.Y. Chung, J.T. Bloking, Y.M. Chiang, Nature Materials 1 (2002) 123–128.
[11] X. Yin, K. Huang, S. Liu, H. Wang, H. Wang, Journal of Power Sources 195 (2010) 4308–4312.
[12] L.J. Li, X.H. Li, Z.X. Wang, H.J. Guo, L. Wu, Y. Hao, J.C. Zheng, Journal of Alloys and Compounds 497 (2010) 176–181.
[13] C.S. Sun, Y. Zhang, X.J. Zhang, Z. Zhou, Journal of Power Sources 195 (2010) 3680–3683.
[14] W.J. Zhou, W. He, Z.M. Li, H.S. Zhao, S.P. Yan, Journal of Solid State Electrochemistry 13 (2009) 1819–1823.
[15] Y. Ren, A.R. Armstrong, F. Jiao, P.G. Bruce, Journal of the American Chemical Society 132 (2010) 996–1004.
[16] T. Nakamura, Y. Shima, H. Matsui, Y. Yamada, S. Hashimoto, H. Miyauchi, N. Koshiba, Journal of the Electrochemical Society 157 (2010) A544–A549.
[17] Z.H. Chen, J.R. Dahn, Journal of the Electrochemical Society 149 (2002) A1184–A1189.
[18] P.S. Herle, B. Ellis, N. Coombs, L.F. Nazar, Nature Materials 3 (2004) 147–152.
[19] K.T. Lee, K.S. Lee, Journal of Power Sources 189 (2009) 435–439.
[20] Y. Lin, M.X. Gao, D. Zhu, Y.F. Liu, H.G. Pan, Journal of Power Sources 184 (2008) 444–448.
[21] M.S. Song, D.Y. Kim, Y.M. Kang, Y.I. Kim, J.Y. Lee, H.S. Kwon, Journal of Power Sources 180 (2008) 546–552.
[22] J.F. Qian, M. Zhou, Y.L. Cao, X.P. Ai, H.X. Yang, Journal of Physical Chemistry C 114 (2010) 3477–3482.
[23] J. Gao, C.Y. Jiang, C.R. Wan, Ionics 16 (2010) 417–424.
[24] D. Zhang, R. Cai, Y.K. Zhou, Z.P. Shao, X.Z. Liao, Z.F. Ma, Electrochimica Acta 55 (2010) 2653–2661.
[25] C. Ho, I.D. Raistrick, R.A. Huggins, Journal of the Electrochemical Society 127 (1980) 343–350.
[26] J. Morales, R. Trocoli, E. Rodriguez-Castellon, S. Franger, J. Santos-Pena, Journal of Electroanalytical Chemistry 631 (2009) 29–35.
[27] M.S. Song, Y.M. Kang, Y.I. Kim, K.S. Park, H.S. Kwon, Inorganic Chemistry 48 (2009) 8271–8275.
[28] Y. Kadoma, J.-M. Kim, K. Abiko, K. Ohtsuki, K. Ui, N. Kumagai, Electrochimica Acta 55 (2010) 1034–1041.
[29] G.T.K. Fey, Y.G. Chen, H.M. Kao, Journal of Power Sources 189 (2009) 169–178.
[30] G.M. Song, Y. Wu, Q. Xu, G. Liu, Journal of Power Sources 195 (2010) 3913–3917.
[31] C.M. Doherty, R.A. Caruso, B.M. Smarsly, C.J. Drummond, Chemistry of Materials 21 (2009) 2895–2903.
[32] Y.Q. Wang, B.L. Wang, J. Yang, Y.N. Nuli, Advanced Functional Materials 16 (2006) 2135–2140.
[33] D.Y.W. Yu, K. Donoue, T. Inoue, M. Fujimoto, S. Fujitani, Journal of the Electrochemical Society 153 (2006) A835–A839.